AIP | Journal of Applied Physics

Self-assembled synthesis and characterization of microchannels in polymeric membranes

Wintana T. Kahsai, Uyen H. T. Pham, Jeyantt S. Sankaran, and Samir M. Iqbal

Citation: J. Appl. Phys. **112**, 024701 (2012); doi: 10.1063/1.4729526
View online: http://dx.doi.org/10.1063/1.4729526
View Table of Contents: http://jap.aip.org/resource/1/JAPIAU/v112/i2
Published by the American Institute of Physics.

Self-assembled synthesis and characterization of microchannels in polymeric membranes

Wintana T. Kahsai,[1,2,3] Uyen H. T. Pham,[1,2,3] Jeyantt S. Sankaran,[1,3,4] and Samir M. Iqbal[1,2,3,4,5,a)]

[1]*Nanotechnology Research & Education Center, University of Texas at Arlington, Arlington, Texas 76019, USA*
[2]*Department of Bioengineering, University of Texas at Arlington, Arlington, Texas 76010, USA*
[3]*Nano-Bio Lab, University of Texas at Arlington, Arlington, Texas 76019, USA*
[4]*Department of Electrical Engineering, University of Texas at Arlington, Arlington, Texas 76011, USA*
[5]*Joint Graduate Studies Committee of Bioengineering Program, University of Texas at Arlington and University of Texas Southwestern Medical Center at Dallas, University of Texas at Arlington, Arlington, Texas 76010, USA*

(Received 4 January 2012; accepted 15 May 2012; published online 19 July 2012)

This article describes a novel self-assembly approach to create microchannels in polydimethylsiloxane (PDMS) membranes using poly(ethylene oxide) (PEO) and polyurethane (PU). The interactions between hydrophilic PEO/PU and hydrophobic PDMS, as it cross-links, result into PEO/PU pushed out of the bulk PDMS. As this occurs, PEO/PU particles leave behind their tracks. PEO depicts ease of handling, better inherent alignment, and excellent repeatability. Fourier transform infrared spectroscopy, optical/confocal laser scanning microscopy, and fluid flow measurements are done to characterize the microfluidic channels. These channels have a circular cross-section and are parallel to each other. PEO generates smaller channels compared to PU. The diameter, arrangement, and height of these channels are seen to depend on temperature; for example, channel length increases linearly with temperature. An interdependent relationship between temperature, pore size, and number of pores is also exhibited. During phase separation of hydrophilic and hydrophobic materials, interface shows concentric circular arrangements of hydrophilic molten polymer. The circular pattern shows almost similar radial change in size. The flow behavior of colored ink solutions shows higher velocity at the entrance of microchannels which decreases to sustained lower velocity as fluid travels farther in the microchannels. The fabrication of membrane does not need lithography or etching, and channels are self-assembled from bottom-up interactions. These microchannel membranes can have applications in drug delivery, cell culture studies, mixing of solutions, separation of mixtures, lab-on-a-chip, etc. © *2012 American Institute of Physics*. [http://dx.doi.org/10.1063/1.4729526]

I. INTRODUCTION

In recent years, uses of polymer microfluidics and separation membranes have grown tremendously. The fluid flow through microchannels and micropores used in miniaturized devices shows interesting properties. Microchannels are fabricated in variety of polymeric materials such as polyurethane (PU), poly(methylmethacrylate) (PMMA), polystyrene, polycarbonate, and polydimethylsiloxane (PDMS). PDMS has received a lot more attention due to low cost and unique properties like transparency, high permeability to gases, high elasticity, easy processing, excellent adhesion to variety of surfaces, hemocompatibility, biocompatibility, etc. It also has biologically relevant Young's modulus.[1–3]

A large amount of work has focused on various techniques for the fabrication of microfluidic devices.[4–10] Photolithography and chemical etching, widely used in microelectronics and microelectromechanical systems (MEMS) patterning, have made soft-lithography the most prevalent technique for PDMS based devices.[11–17] The constraints on such fabrication techniques are that these are expensive, time consuming, complicated, and require specialized tools. Furthermore, the end results of these approaches are mostly rectangular shaped channels.[18–20] These types of channels are not desirable for certain applications such as deformable membrane based valves sealing, sealing between a cell and microchannel opening, or to mimic microcirculation of blood.[21–23] Normal cell growth can easily be affected and cell growth may even stop due to varying shear stresses that can form at the corners of rectangular channels. Circular cross-sectioned microchannels are, therefore, more appropriate for microfluidics-based electromechanical studies of living cells, like those employed in micropipette aspiration.[24]

Recently, novel approaches of microchannel fabrication in PDMS membrane using self-assembly have been reported. Self-assembled polymeric particles were shown to result into nanochannels due to entropic and enthalpic changes in the system.[25,26] In polymers like PDMS, the decrease of entropy is a result of polymerization, which reduces number of configurations that molecular sub-units can have.[27–29] During polymerization, the cross-linking reaction decreases the

a)Author to whom correspondence should be addressed. Electronic mail: smiqbal@uta.edu.

entropy of the system. The macromolecular network extends to the whole sample and coexists with loose branched networks that are not yet part of the network. A crossover in the liquid to solid phase of the polymer is called the gel-point.[25] Now if there are hydrophilic particles in a hydrophobic polymer like PDMS, these particles do not get intercalated during gelation.[30] The method of fabrication presented in this article is based on this idea where repulsion forces at the hydrophilic-hydrophobic interfaces are used to influence the immiscible particles to be pushed out of PDMS during polymerization. The applied heat decreases the mobility of cross-linking sub-units and gelation reduces entropy of the system while PDMS is cross-linked. This phenomenon results for the system to self-assemble hydrophilic molecules to go from bottom to up in such a way that hollow microchannels are formed.

The fabrication of microchannels with self-assembly provides a rapid and efficient approach that does not require any special equipment, and results in circular microchannels. This article focuses on fabrication of poly(ethylene oxide) (PEO) and polyurethane (PU) induced circular microchannels, based on using the natural force of repulsion between hydrophobic and hydrophilic materials (Fig. 1).

PEO and PU were used as powder and beads, respectively. The particles of these materials were used to generate microchannels through PDMS membrane. When the hydrophilic particles came in contact with hydrophobic PDMS and were exposed to heat, PDMS started to polymerize from bottom to top creating tight networks of localized chains. This phenomenon is called "curing". As the PDMS liquid cured and turned into solid, hydrophilic particles migrated from bottom to the top leaving hollow channels behind. Formation of channels was a result of energy transferred through the heat leading to higher entropy of hydrophilic particles plus phase separation due to force of repulsion at the interface between hydrophobic and hydrophilic materials. Random movement and collision of particles occurred when the hydrophilic microparticles were exposed to heat. Temperature played a key role by changing the physical state of the hydrophilic particles and in the process increasing their entropy. However, during polymerization, when the temperature increased, the entropy of PDMS decreased.[25] Entropy of a system is given by:

$$\Delta S = \Delta S_f - \Delta S_i, \tag{1}$$

where ΔS is change in the entropy of a system, ΔS_f and ΔS_i are the final and initial entropies, respectively. The reduction in possible configurations a growing network of PDMS could take, prevented PDMS from closing back the hollow space formed by the migration of hydrophilic particles and secured the formation of channels.

Characterization of channels was done with respect to temperature, positioning of hydrophilic particles and fluid flow properties like velocity of fluid and mixing of two fluids inside channels. The fluid flow was driven using capillary electrophoresis only.

II. EXPERMENTAL METHODS

A. Fabrication of microchannels

Commercial grade PEO powder and PU beads, both hydrophilic in nature, were used in the experiments. PEO powder was composed of microparticles and PU bead sizes were between 2.5 and 3.5 mm. PDMS was prepared by using Sylgard 184 kit which consisted of PDMS base and curing agent. The base was mixed with the curing agent in a ratio of 10:1 and stirred vigorously for several minutes until the curing agent was homogeneously distributed. Degassing was performed by placing the mixture in a vacuum chamber at 30 psi until all trapped air was removed. Ten micrograms of the PEO microparticles were placed spread out in a Petri dish at temperature between 200 and 400 °C. At these temperatures, PEO microparticles completely transitioned to molten and viscous fluid within a few seconds and started to evaporate. PDMS (2–3 g) was poured on top of the viscous PEO film. The opposite affinities of PEO and PDMS made pouring of PDMS very critical. The pouring of PDMS in the Petri dish on top of the molten PEO was thus a key step which influenced the final sizes and positions of microchannels. When PDMS was poured from one side to another by gradually laying it over the Petri dish, the viscous film was not disturbed and initial position remained intact. On the other hand, if PDMS was poured at just one position spreading in expanding puddle pattern, the molten PEO moved away from the center. The different characteristics of microchannels evolved as a result of different pouring techniques.

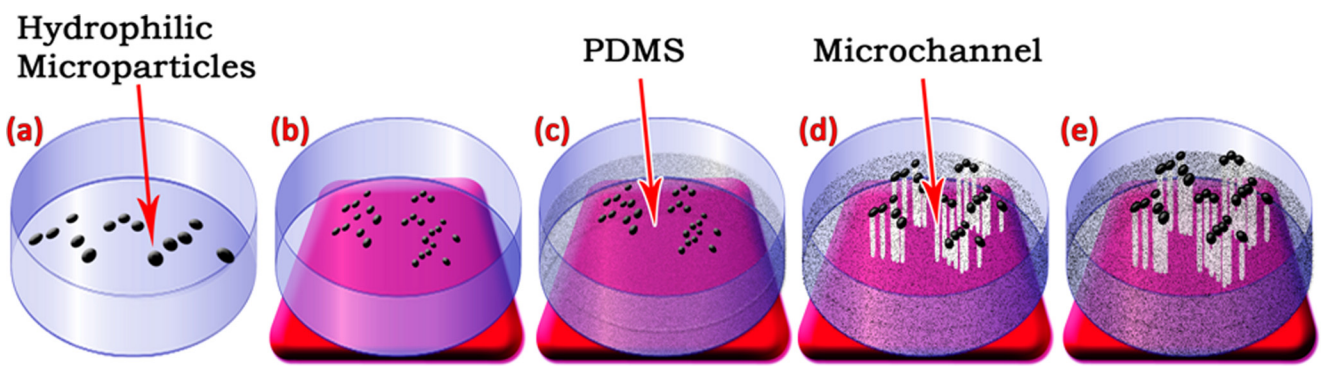

FIG. 1. Schematics depicting steps of microchannel fabrication in PDMS using hydrophilic particles. Red plate denotes hotplate. (a) Hydrophilic particles in Petri dish before exposure to heat; (b) hydrophilic particles after expose to heat; (c) PDMS poured on top of hydrophilic particles; (d) PDMS starts to polymerize and hydrophilic particles migrate forming microchannels along the way; (e) PDMS fully polymerizes with *in situ* growth of microchannels.

Polymerization process took from a few seconds to about 2 minutes depending on the temperature used. Once PDMS was fully polymerized, the Petri dish was removed from the hotplate and was allowed to cool down to room temperature. Experiments for PU beads were done in a similar manner. About 6–8 beads of PU were used for each experiment. Both of these hydrophilic materials generated hollow channels closed at both ends. For characterization, channels were sliced open to measure pore sizes. These were also sliced from top to bottom to measure the length of channels. Confocal and optical micrographs of channels were taken and analyzed. Furthermore, Fourier transform infrared (FTIR) spectra were measured for PEO, PU, pure PDMS, and the porous membranes fabricated with both PEO and PU.

B. Fluid flow

The fabricated microchannels were treated with oxygen plasma for 15 min for characterization of fluid flow using capillary action. First experiment was carried out by opening only one side of the channels. The open side of the channel was placed down inside a blue ink solution. Once the fluid got sucked up in the channels of membrane, the membrane was removed from blue solution and placed in a red ink solution.

In second set of experiments, channels were cut open from both sides and membrane was placed horizontally. Red and blue ink drops were placed on opposite ends of the channels using a syringe.

In third class of experiments, a 300 μm channel was cut open from both sides and a red drop was placed on one opening using a syringe. The capillary action sucked in the fluid. This time was defined as $t = 0$. The fluid motion was observed with optical microscope. The velocity of fluid inside microchannel was calculated by measuring distance traveled in unit time and flow rate was analyzed.

III. RESULTS AND DISCUSSION

A. Characterization of surface chemistry

Figure 2 shows FTIR spectra of PEO, PU, pure PDMS, and membranes formed by interactions of PEO and PU with PDMS. PEO and PDMS are polymers with molecular structure HO-CH_2-(CH_2-O-CH_2-)$_n$-CH_2-OH and $CH_3[Si(CH_3)_2O]_n$ $Si(CH_3)_3$, respectively. The most concentrated absorption peaks for PDMS are at 387 cm^{-1} attributed to Si-O rocking mode, 791 cm^{-1} to Si-CH_3 bending mode, 1014 cm^{-1} to Si-O stretching vibration, 1258 cm^{-1} to -Si-CH_3 stretching vibration, and 2958 cm^{-1} to –CH_3 asymmetric stretching mode.[31,32] The peak at 1113 cm^{-1} indicates C-O stretching, the one at 2889 cm^{-1} relates to –CH_2 stretching vibration and 1470 cm^{-1} is from –CH_2 scissor, all inherent to PEO only. It is important to note that PDMS membranes fabricated using PEO or PU show vibration modes associated with PDMS only (Fig. 2). This shows the absence of PEO and PU from the porous membrane after generating the channels. The results indicate that bulk and pure PDMS and porous PDMS membranes fabricated using either PEO or PU have similar FTIR data, whereas PEO and PU have absolutely different peak profile. The porous membranes were thus composed of PDMS only and no contamination or intercalcation of other polymers was seen.

B. Characterization of porosity and pore size

Figs. 3(a) and 3(b) show channels formed in PDMS driven by PEO and PU, respectively. Circular contoured pore formation is apparent from the cross-sectional photomicrographs. Side views of hollow microchannels that are closed from both ends are also shown in the insets of Figs. 3(a) and 3(b). The channels generated using PEO tended to depict smaller diameters than PU particles. At 300 °C, PU driven channels had diameters almost twice of those for PEO

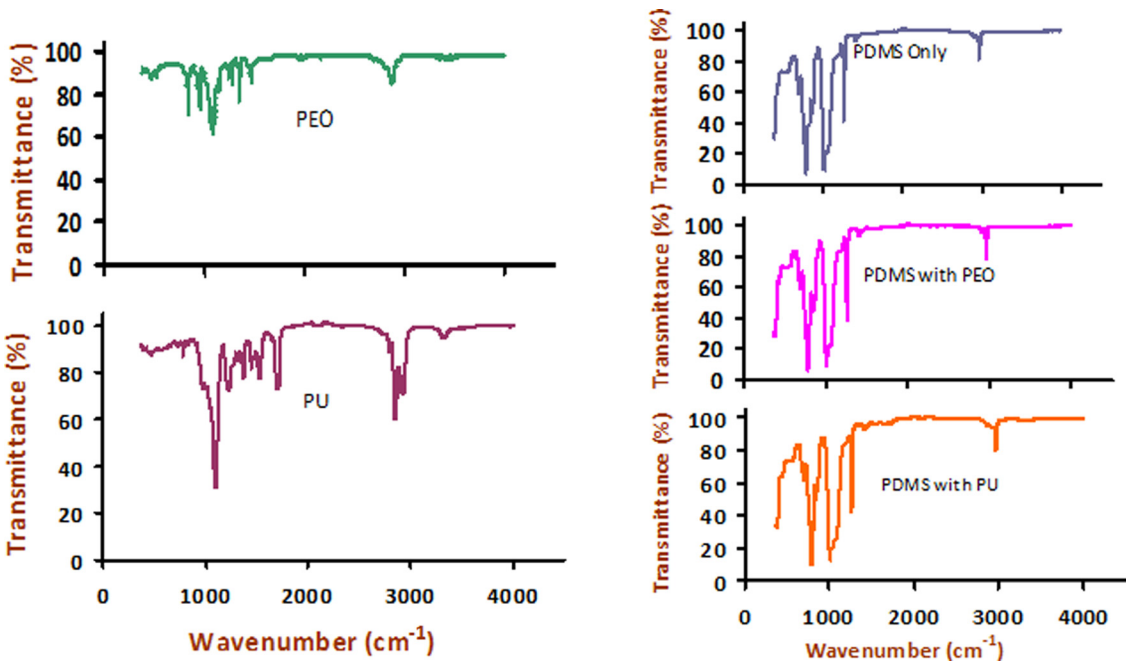

FIG. 2. FTIR spectra of PEO, PU, PDMS only, and PDMS membranes fabricated using PEO and PU.

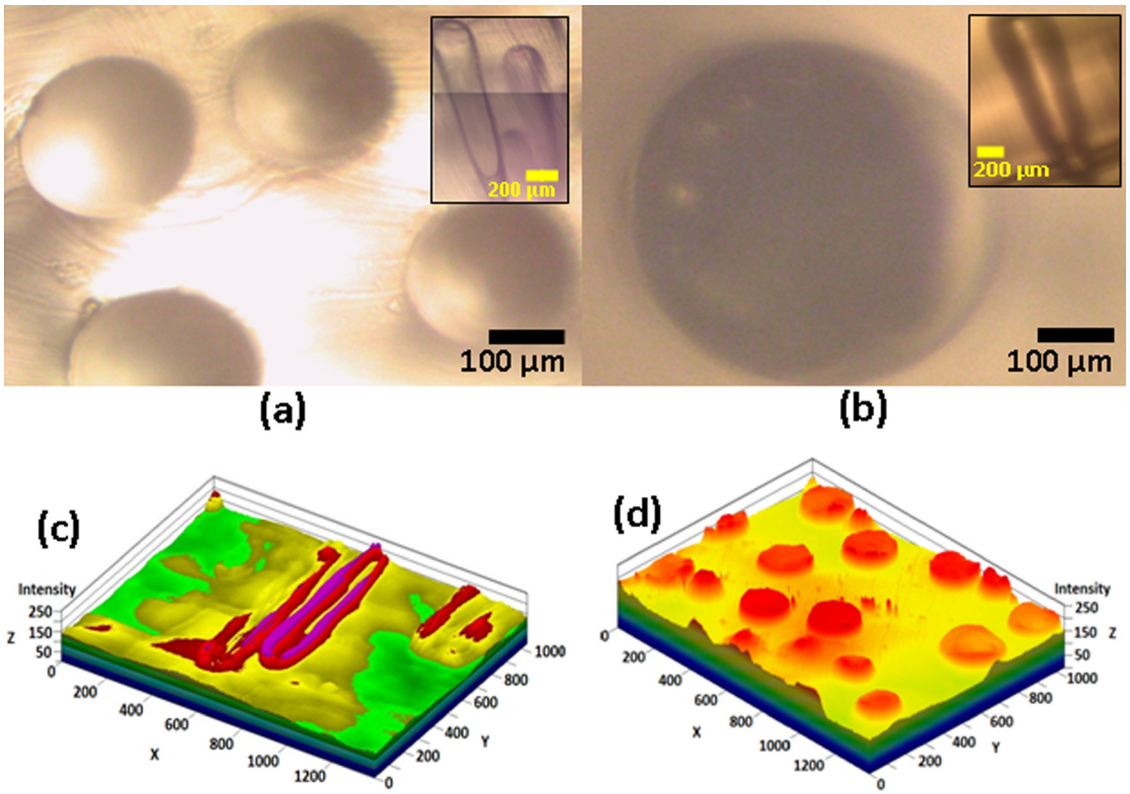

FIG. 3. Microchannels in PDMS made with (a) PEO and (b) PU. Insets of (a) and (b) show the lengths of the microchannels. Confocal laser scanning microscope (CLSM) micrographs of PEO driven channels: (c) Shows cross-section along the channel length while (d) shows top view. The x,y, and z-axis units are arbitrary.

driven channels. After melting the polymers at 300 °C, PU was more viscous than PEO. The inter-molecular force of attraction is known to be weaker for less viscous solutions. Therefore, when PDMS was poured on top of PEO, the weaker attraction between PEO molecules resulted into smaller clusters that resulted in smaller but many more microchannels, in contrast to PU induced channels. PU, on the other hand, was much more viscous than PEO and formed fewer and bigger clusters resulting in larger channel diameters. Figs. 3(a) and 3(b) exhibit the higher number of smaller channels formed for PEO than PU.

C. Temperature dependence

The porosity of the membrane and the PDMS pore sizes also showed a dependence on the curing temperature. The data in Fig. 3(c) show presence of short channels (at the right corner) as well as long channels that travel all the way to the top (the two channels in the middle). Due to this variation in channel lengths, results of porosity varied depending on the level where membrane was cross-sectioned to measure pore sizes and porosity. The results of Table I show data close to the bottom of the membrane where pores were smaller. There were many more pores at this level than at the top (Fig. 4) due to the fact that not all pores made it all the way to the top (also seen in Fig. 3(c)). The trend of Table I shows that when PDMS membranes were cured at higher temperature, the pore sizes decreased and number of pores increased. The smallest diameter was recorded at the highest temperature. At higher temperatures, the intermolecular bonds were weak and solution became less viscous. This formed smaller but many more clusters that resulted in many more channels formed with much smaller diameters. However, towards the top of the membranes, the pore sizes increased and porosity reduced. Fig. 4 shows the channels cross-sectioned close to the top surface. This data showed characteristics of the long channels only. Here, it can be seen that both the pore size and porosity increased with increasing temperature. The data of Table I and Fig 4(a), although seemingly contradictory, in fact show that at the bottom of the membrane (Table I), the pore sizes were smaller for higher temperatures. Towards the top of the membrane, the pore sizes became larger (Fig. 4(a)). This depicted funnel shaped pores at higher temperatures, with sizes of the top openings of pores made at all temperatures to be within 10%-15% of the sizes of the pores made at 400 °C. But the channel sizes at lower levels varied considerably with curing temperature.

Figure 5 shows the distinct arrangements of microchannel resulting from the two approaches undertaken to disperse PDMS pre-polymer. PEO polymers clustered to form

TABLE I. Relationship between temperature, porosity, and pore size at cross-sections close to the bottom.

Temperature (°C)	No. of pores	Average pore size (μm)
225	0	0 ± 0
250	3	69 ± 1.2
275	13	60 ± 16
300	38	34 ± 11

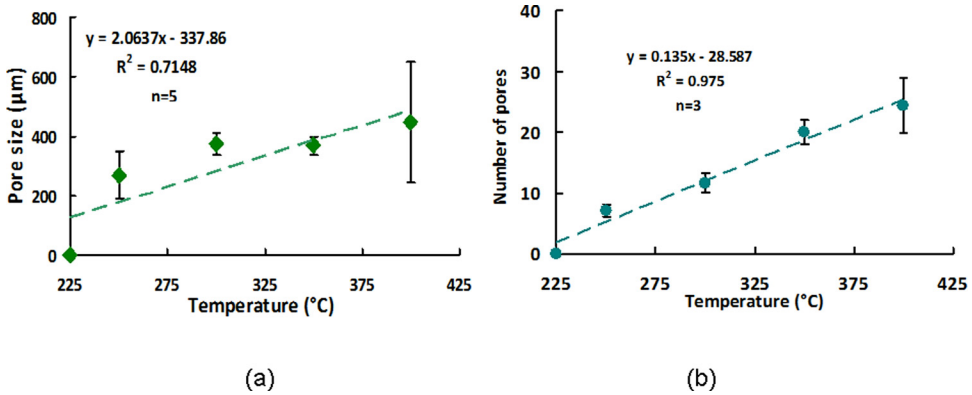

FIG. 4. Effects of temperature on (a) average pore size and (b) Porosity measured at the top of the membranes.

micelles when these came in contact with PDMS. PU exhibited similar reactions. Micellar shapes are common because of hydrophilic/hydrophobic interactions.[33,34] After melting PEO or PU, PDMS was gradually poured on top of these hydrophilic molecules from one end to another. This kept hydrophilic particles intact in their original positions (Figs. 5(a) and 5(b)) and led to formation of microchannels that were in close vicinity localized in confined area. However, when PDMS was poured in a way that disturbed the original arrangement, channel formation was positioned in two ways. When hydrophilic particles were not completely molten, the solution moved as small streams and branched to form channels (Fig. 5(c)). At times when the hydrophilic particles were completely molten and spread in a large area, the channels were generated along the lines where hydrophilic and hydrophobic molecules interfaced each other (Figs. 5(d) and 5(e)).

When PDMS was continuously poured at just one point, the viscous hydrophilic PEO polymer was pushed in an expanding circle fashion forming concentric rings. This was a result of phase separation when the two repulsive molecules, hydrophilic molten PEO and growing networks of hydrophobic PDMS, came in contact. When the mixtures have repulsive forces toward each other, the separation of the two species into two distinct macroscopic phases is favored.[35] Due to the way the PDMS was poured, the hydrophilic molten clusters were phase separated in unique way. When PDMS polymerized, several horizontal, continuous and concentric rings were formed at almost equal difference

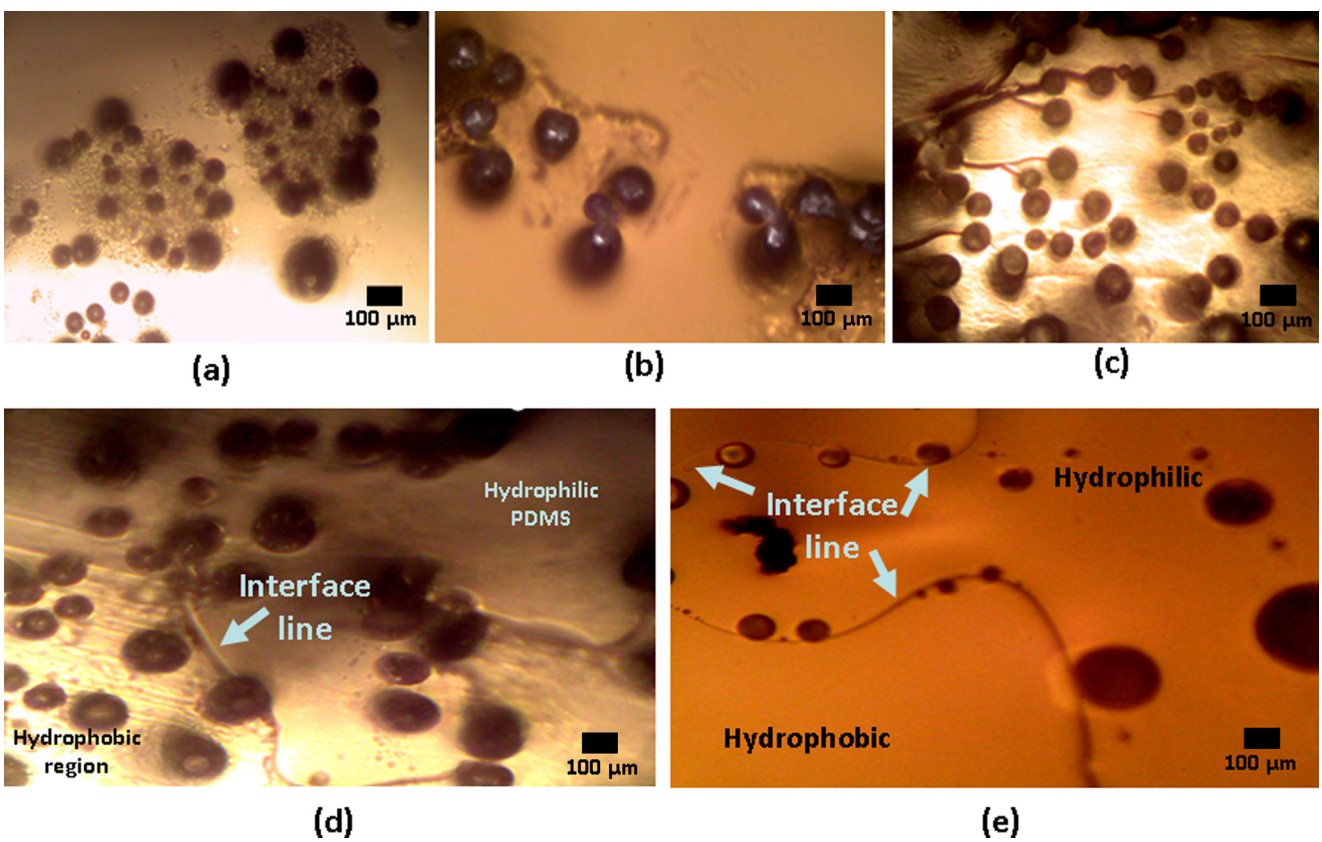

FIG. 5. Microchannel arrangements at hydrophilic–hydrophobic interface. (a) PDMS poured gradually without disturbing initial placement of PEO particles. (b) PDMS poured gently without disturbing initial position of PU particles (c) When hydrophilic particles are not molten completely these form thin dendrite like branches forming into channels. (d) Channel formations at the interface line when PEO melts completely and (e) channel formations at the interface line when PU particles melt completely.

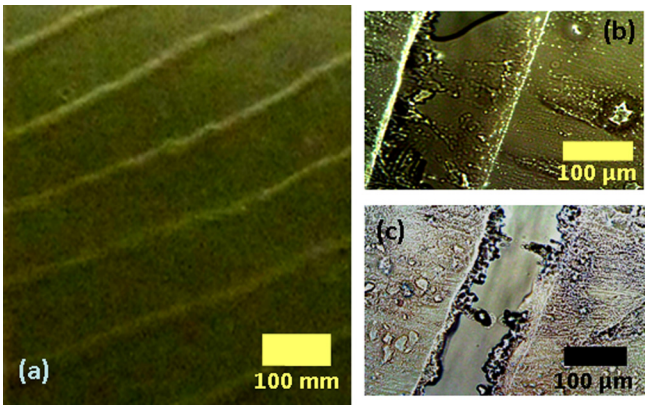

FIG. 6. (a) Concentric rings of hollow space formed when PDMS is poured over molten PEO. (b) A magnified view of a single closed hollow space formed. (c) A magnified view of a single opened hollow space formed.

in diameters (Fig. 6(a)). This method also formed channels that were farther away from each other since particles pushed along the growing rings. Some of these rings were closed hollow channels while some were open (Fig. 6(b) and 6(c)).

D. Characterization of channel lengths

Temperature showed a strong effect on the channel lengths. Hydrophilic materials were more mobile when PDMS was in its viscous form. When the system was exposed to heat, entropy of these particles increased and these started to move upward while entropy of PDMS decreased due to formation of cross-linked gel like solid. There was no channel formation when temperature was less than 200 °C. At 225 °C, there were few round dent like structures (Fig. 7(a)). At temperatures above 250 °C, full blown channels appeared. The channels were larger at higher temperatures (Figs. 7(b) and 7(c)). An almost linear relationship between channel length and temperature is visible in Fig. 8. At lower temperatures, channel formation was slower compared to the rate of polymerization. Once cross-linking was completed and whole mass of PMDS was polymerized, formations of channels stopped leading to shorter channel formation. When the curing temperature went from 250 °C to

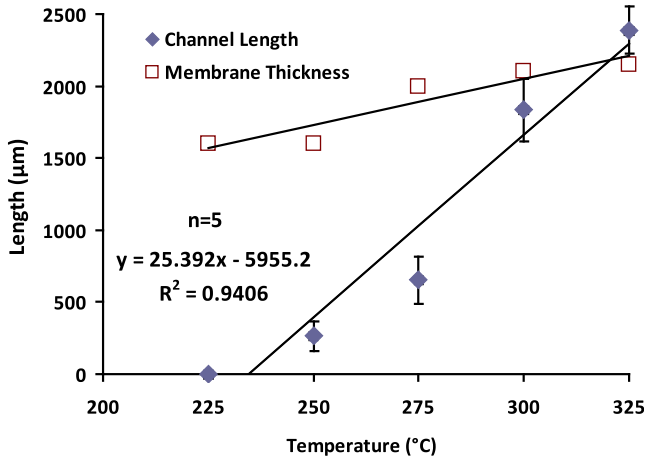

FIG. 8. Channel length vs. temperature. Increasing the curing temperature results into longer channels.

325 °C, the average channel lengths increased dramatically from 600 μm to 2274 μm.

An interesting phenomenon was observed at 325 °C where the channel length surpassed the thickness of the membrane. At this temperature, the hydrophilic particles gained plenty of energy from the temperature such that some channels stretched above the top of the membrane (Fig. 7(c)). PDMS, being elastic, let these channels sprout above the thickness of the membrane, contained within a thin film of PDMS.

E. Capillary action driven fluid flow

Capillary effect-driven fluid flow experiments showed the integrity and micromixing capabilities of the microchannels. Micromixing of solution was done without any external force. Capillary force (F_C) transferred fluid inside microchannel based on the diameter of channels (D), surface tension (σ), and contact angle (θ). F_C is given by:[36]

$$F_C = \sigma \cos\theta \pi D. \tag{2}$$

Plasma treated microchannels with 250 μm diameter were cut open from both ends and exposed to red ink and blue ink

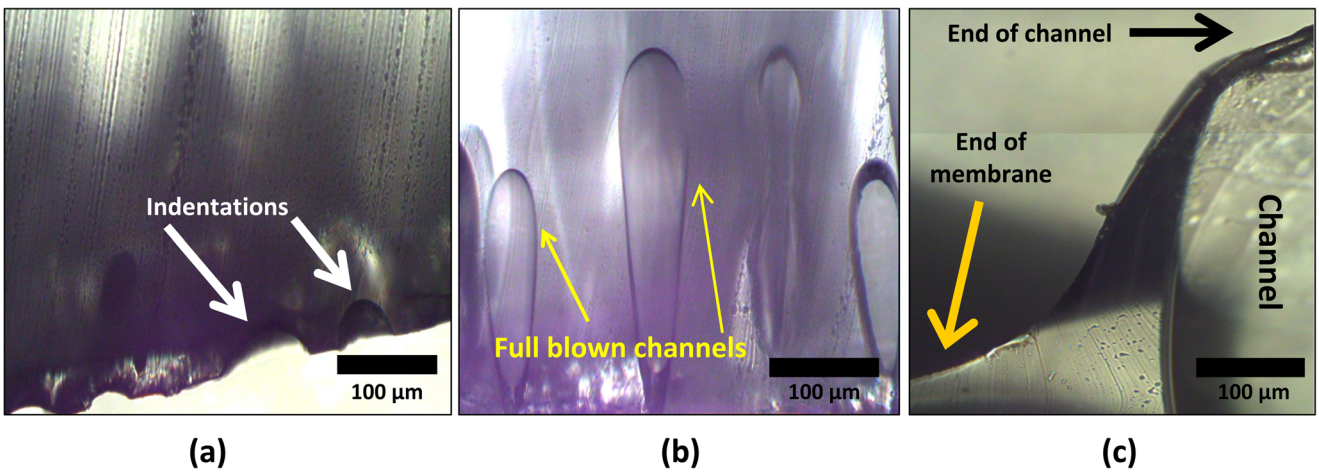

FIG. 7. Side view of channels formed at different temperatures. (a) At 225 °C, there are only dent like formations. (b) Formation of microchannels at 250 °C. (c) Channel stretch out above the top of the membrane at 325 °C.

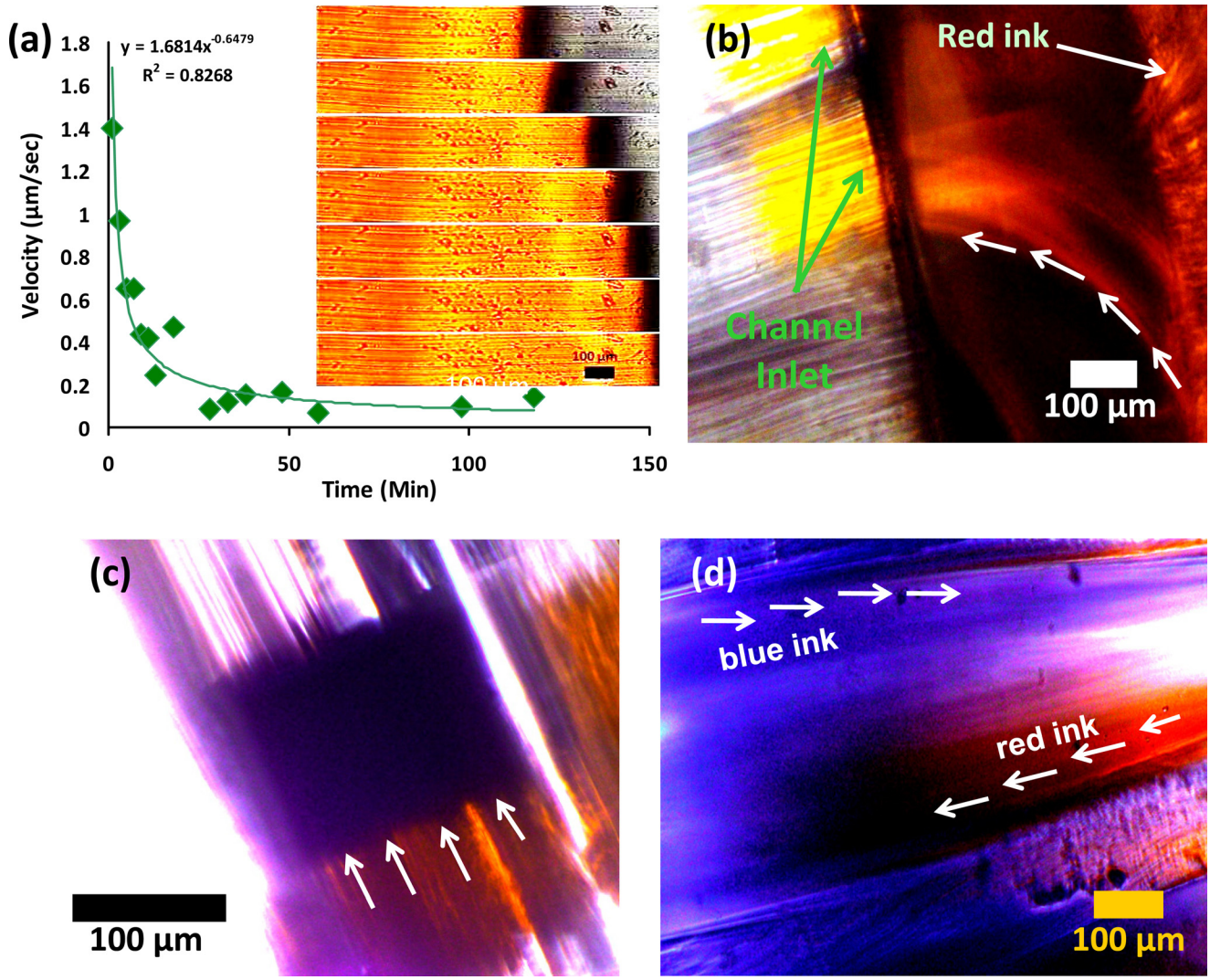

FIG. 9. The flow of fluid inside microchannels. (a) Plot shows decrease in fluid flow velocity with time. Inset shows time lapse photomicrographs of red ink moving under capillary force. (b) Capillary force pulling fluid into the channels. The arrows show the direction of fluid flow. (c) Red ink flowing through adjacent channels. Red ink is following blue ink in the left channel whereas there is no blue ink in the right channel (partially visible). (d) Mixing of red and blue fluids by using capillary force from opposite inlets.

from two sides. Optical microscope was used to measure distance of fluid traveled over time which enabled calculation of fluid flow velocity inside the channels. Fig. 9(a) inset shows optical photomicrographs of fluid flow inside microchannel with respect to time. Distance of the flow was measured along the channel axis. Velocity was high at the onset of flow and started to decrease with distance and got stabilized after certain time. When fluid flowed from wide area to a narrow constricted area, velocity should have increased in order to maintain a constant flow rate but was seen to decrease.[37] There are surface charges on PDMS that may have contributed to counter-intuitive observations. Velocity (V) was calculated using Lagrangian description which states the motion of a differential fluid volume using fixed reference frame. Velocity was measured as rate of change of position of fluid (dx) with respect to time (dt):

$$V = dx/dt. \tag{3}$$

At the entrance of the microchannels, the initial velocity was 6.25 μm/s. For the first two minute, the velocity was maintained but then it dropped gradually. It went down to1.4 μm/s and then became as small as 0.085 μm/s in 30 min.

Fig. 9(b) shows a strong capillary force pulling the fluid into the microchannels even when the channel inlet was physically away from the level of the fluid. Fig. 9(c) demonstrates the two fluids flowing through one inlet. The advantages of using this system were that the microchannel fabricated was capable of capillary action, and PDMS being permeable to gases showed no trapped air between the two solutions (Fig. 9(c)). This can be important for well-based immunoassays and simultaneous detection systems which is difficult to perform in traditional well-plate systems. Figure 9(d) shows results for the solutions that were placed at opposite openings of the channel. The two solutions migrated from both sides toward each other. Fusion and mixing of the two solutions are evident at the middle of the channel.

IV. CONCLUSIONS

A self-assembled approach to synthesize circular microchannels ranging from few μm to hundreds of micrometers is

demonstrated using simple interplay of hydrophilic and hydrophobic polymers. The formed microchannels were characterized for chemical composition, size, porosity, and fluid flow. FTIR results showed that PEO or PU traces were not detected in the porous PDMS membranes. PEO hydrophilic particles generated smaller pores compared to PU beads. The size distribution of the channels could be controlled by controlling pouring of PDMS. Channels in close vicinity were generated when PDMS was poured without disturbing the molten viscous hydrophilic films. But, when PDMS was poured at one position, it spread in expanding circle shape dislocating the original position of hydrophilic particles along the way. This resulted in concentric circular distribution of PEO at almost equal distances apart and thus formation of channels in concentric circles. Various channel lengths were fabricated by controlling the thickness of membrane and temperature. Fluid flow inside the channels was also characterized by measuring velocity change over time.

ACKNOWLEDGMENTS

The authors acknowledge useful discussion with Swati Goyal, Brian Edwards, Waseem Ashgar, Abdul A. N. Mohammed, Chaudhry M. A. Arafat, and Nahum Torres-Arenas. This work was supported by National Science Foundation CAREER Grant (ECCS-0845669) to SMI. W. T. Kahsai and J. S. Sankaran also acknowledge support by Travel Fellowships from Consortium for Nanomaterials for Aerospace Commerce and Technology (CONTACT) Program, Rice University, Houston, TX, USA.

[1]C. Fidkowski, M. R. Kaazempur-Mofrad, J. Borenstein, J. P. Vacanti, R. Langer, and Y. Wang, Tissue Eng. **11**, 302–309 (2005).
[2]H. Hufnagel, A. Huebner, C. Gulch, K. Guse, C. Abell, and F. Hollfelder, Lab Chip **9**, 1576–1582 (2009).
[3]H. Makamba, J. H. Kim, K. Lim, N. Park, and J. H. Hahn, Electrophoresis **24**, 3607–3619 (2003).
[4]C. J. Campbell, R. Klajn, M. Fialkowski, and B. A. Grzybowski, Langmuir **21**, 418–423 (2005).
[5]S. Masuda, M. Washizu, and T. Nanba, IEEE Trans. Ind. Appl. **25**, 732–737 (1989).
[6]B. D. DeBusschere, D. A. Borkholder, and G. T. A. Kovacs, "Design of an integrated silicon-PDMS cell cartridge," in *Proceedings of the Solid-State Sensor and Actuator Workshop, Hilton Head, South Carolina, June 8–11, 1998*, IEEE, pp. 358–362.
[7]A. Liu, F. He, K. Wang, T. Zhou, Y. Lu, and X. Xia, Lab Chip **5**, 974–978 (2005).
[8]J. C. McDonald and G. M. Whitesides, Acc. Chem. Res. **35**, 491–499 (2002).
[9]D. W. L. Tolfree, Rep. Prog. Phys. **61**, 313 (1998).
[10]H. Wu, T. W. Odom, D. T. Chiu, and G. M. Whitesides, J. Am. Chem. Soc. **125**, 554–559 (2003).
[11]Y. Cheng, K. Sugioka, and K. Midorikawa, Appl. Surf. Sci. **248**, 172–176 (2005).
[12]Y. Kikutani, T. Horiuchi, K. Uchiyama, H. Hisamoto, M. Tokeshi, and T. Kitamori, Lab Chip **2**, 188–192 (2002).
[13]I. Schneega, R. Brautigam, and J. M. Kohler, Lab Chip **1**, 42–49 (2001).
[14]M. Abdelgawad, M. W. L. Watson, E. W. K. Young, J. M. Mudrik, M. D. Ungrin, and A. R. Wheeler, Lab Chip **8**, 1379–1385 (2008).
[15]S. K. Sia and G. M. Whitesides, Electrophoresis **24**, 3563–3576 (2003).
[16]M. A. Unger, H. P. Chou, T. Thorsen, A. Scherer, and S. R. Quake, Science **288**, 113 (2000).
[17]J. P. Urbanski, W. Thies, C. Rhodes, S. Amarasinghe, and T. Thorsen, Lab Chip **6**, 96–104 (2006).
[18]M. J. Fuerstman, A. Lai, M. E. Thurlow, S. S. Shevkoplyas, H. A. Stone, and G. M. Whitesides, Lab Chip **7**, 1479–1489 (2007).
[19]M. T. Koesdjojo, Y. H. Tennico, J. T. Rundel, and V. T. Remcho, Sens. Actuators B **131**, 692–697 (2008).
[20]G. B. Lee, C. C. Chang, S. B. Huang, and R. J. Yang, J. Micromech. Microeng. **16**, 1024 (2006).
[21]S.-H. Song, C.-K. Lee, T.-J. Kim, I.-C. Shin, S.-C. Jun, and H.-I. Jung, Microfluid. Nanofluid. **9**, 533–540 (2010).
[22]J. Borenstein, M. Tupper, P. Mack, E. Weinberg, A. Khalil, J. Hsiao, and G. García-Cardeña, Biomed. Microdevices **12**, 71–79 (2010).
[23]J. P. Camp, T. Stokol, and M. L. Shuler, Biomed. Microdevices **10**, 179–186 (2008).
[24]M. Abdelgawad, C. Wu, W.-Y. Chien, W. R. Geddie, M. A. S. Jewett, and Y. Sun, Lab Chip **11**, 545–551 (2011).
[25]J. S. Sankaran, S. Goyal, W. T. Kahsai, U. H. T. Pham, and S. M. Iqbal, Adv. Sci. Lett. **4**, 3464–3469 (2011).
[26]K. Venumadhav *et al.*, Nanotechnology **20**, 425602 (2009).
[27]J. F. Paul and John Rehner, Jr., J. Chem. Phys. **11**, 521–526 (1943).
[28]P. J. Flory and W. R. Krigbaum, Annu. Rev. Phys. Chem. **2**, 383–402 (1951).
[29]J. S. Sankaran, W. T. Kahsai, U. H. T. Pham, and S. M. Iqbal, "Lithography-Free Microchannel Fabrication in PDMS," in *Bulletin of the American Physical Society, APS March Meeting 2011, Volume 56, Number 1, March 21–25, 2011,* Dallas, Texas.
[30]R. Krishnamoorti, R. A. Vaia, and E. P. Giannelis, Chem. Mater. **8**, 1728–1734 (1996).
[31]K. Maex, M. R. Baklanov, D. Shamiryan, S. H. Brongersma, and Z. S. Yanovitskaya, J. Appl. Phys. **93**, 8793 (2003).
[32]C. C. Yang, P. T. Wu, W. C. Chen, and H. L. Chen, Polymer **45**, 5691–5702 (2004).
[33]W. Brown, K. Schillen, M. Almgren, S. Hvidt, and P. Bahadur, J. Phys. Chem. **95**, 1850–1858 (1991).
[34]P. Alexandridis, J. F. Holzwarth, and T. A. Hatton, Macromolecules **27**, 2414–2425 (1994).
[35]R. O. Prum, E. R. Dufresne, T. Quinn, and K. Waters, J. R. Soc., Interface **6**, S253 (2009).
[36]N. Ichikawa, K. Hosokawa, and R. Maeda, J. Colloid Interface Sci. **280**, 155–164 (2004).
[37]G. A. Truskey, F. Yuan, and D. F. Katz, *Transport Phenomena in Biological Systems* (Pearson/Prentice Hall, New Jersey, 2004).